Free-carrier mobility in GaN in the presence of dislocation walls

J.-L. Farvacque,[1] Z. Bougrioua,[2] and I. Moerman[2]
[1]*Laboratoire de Structure et Propriétés de l'Etat Solide, Université des Sciences et Technologies de Lille, CNRS ESA 8008, 59655 Villeneuve d'Ascq cedex, France*
[2]*Department of Information Technology, IMEC, Ghent University, Sint-Pietersnieuwstraat 41, 9000 Ghent, Belgium*
(Received 5 July 2000; published 27 February 2001)

The free-carrier mobility versus carrier density in *n*-type GaN grown by low-pressure metal-organic vapor-phase epitaxy on a sapphire substrate experiences a particular behavior that consists of the appearance of a sharp transition separating a low- from a high-mobility regime. This separation appears as soon as the carrier density exceeds a critical value that depends on the growth process. Using low-field electrical transport simulations, we show that this particular mobility behavior cannot be simply interpreted in terms of dislocation scattering or trapping mechanisms, but that it is also controlled by the collective effect of dislocation walls (the columnar structure). As the free-carrier density increases, the more efficient screening properties result in the transition from a barrier-controlled mobility regime to a pure-diffusion-process-controlled mobility regime. The model permits us to reproduce the experimental mobility collapse quantitatively.

DOI: 10.1103/PhysRevB.63.115202 PACS number(s): 72.10.Fk, 72.80.Ey

I. INTRODUCTION

The promising possibilities of GaN for advanced electronic devices operating at high temperature and high power density have recently raised some attention for the experimental and theoretical studies of its transport properties. In practice, GaN layers are mainly grown using the metal-organic vapor-phase epitaxy (MOVPE) technique on highly lattice-mismatched sapphire substrates. Thus, as evidenced by transmission electron microscopy (TEM) observations, bulk material is, in the state of the art, generally characterized by very large dislocation densities (typically in the range 10^8 to mid-$10^{10}\,cm^{-3}$) more or less arranged in walls: the so-called ''columnar cell'' structure. In such material, the room-temperature carrier mobility measured experimentally has often been found to be extremely low at a low *n*-type doping level while it reaches standard values for larger doping. This behavior is singular when compared to the classical behavior that shows that the carrier mobility is mainly controlled by phonon and ionized impurity scattering, and as a consequence the lower the doping level the larger the carrier mobility.[1–4] In our case, the mobility versus carrier density presents an even clearer trend as it displays a sharp transition, which separates a low-mobility regime as long as the carrier density is lower than a critical value, from a large-mobility regime (the so-called mobility collapse in Refs. 5 and 6). This particular behavior has been seen in several series of samples grown by low-pressure (LP) MOVPE using the two-step procedure described in Refs. 7 and 8.

Figure 1 shows an example of two sets of experimental points corresponding to two families of layers grown with two different growth processes: the transitions occur at about 8×10^{17} and $2\times10^{17}\,cm^{-3}$, respectively, for series α and series Ω. For each series, the only variable parameter is the concentration of the Si dopant (diluted silane), so samples belonging to a given series are expected to possess quite identical defect substructures. Our experimental procedure allows us to eliminate the result dispersion found in literature. TEM observations[5,9] indicate that any of our samples is, as usually, characterized by a columnar cell structure constituted by threading dislocations more or less arranged in walls (rough subgrain boundaries). A rough estimate of the dislocation density is about 2×10^{10} and $5\times10^{9}\,cm^{-3}$, respectively, for series α and series Ω. It is found that varying the growth conditions in order to improve the crystalline quality of the material leads to a smaller value of the critical carrier density at which the steep transition in transport regime occurs. This transition is likely to be a fingerprint of the material microstructure quality.

In order to understand the low-mobility regime in *n*-type GaN layers, numerous theoretical simulations of the transport properties including the dislocation scattering mechanisms have been undertaken.[5,6,10–14] All of them converge to claim that dislocations do actually strongly affect the mobility at low temperature and/or at low carrier density. However classical transport approaches remain quite unable to describe the sharp collapse of the mobility versus the free carrier density for a given temperature. In Refs. 5 and 6, we have already reported that this behavior cannot be described by assuming that dislocations only act as scattering centers. In the present paper, we qualitatively and quantitatively show that it results from the presence of dislocation walls

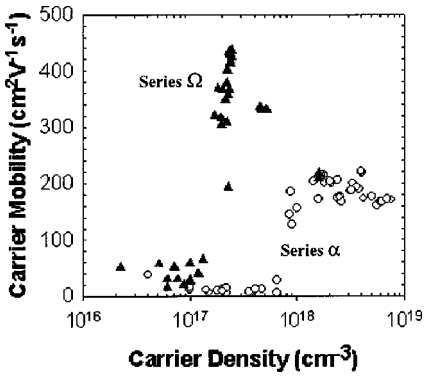

FIG. 1. Evolution of the 300-K Hall carrier mobility as a function of the Hall carrier density for two sets of GaN layers: series α (white circles) and series Ω (black triangles), each grown with a specific growth process (Ref. 8).

(i.e., the dislocation substructure), which act as electronic barriers as long as the screening properties of the material remain quite unable to separate the energy band bending associated with in-wall-neighboring dislocations.

II. TRANSPORT ANALYSIS IN TERMS OF DIFFUSION PROCESS

A. The theoretical frame of the present simulation

The most recent works found in literature[1–4,10–14] concerning low-field transport analysis of GaN have been mainly performed in the frame of the relaxation time concept, which, in principle, may only be defined in the particular case of *isotropic* and *elastic* scattering mechanisms.[15] GaN contains a very large dislocation density and is also characterized by a very large energy of the optical phonons (91 meV). However, in this case also we expect that the carrier mobility will strongly depend on (i) the dislocation content, which is a typical example of an *anisotropic* scattering center, and on (ii) optical phonon scattering mechanisms, which are the prototype of *inelastic* scattering mechanisms. Even if the use of the relaxation time may be extended to such cases as an approximation, we preferred to ground our own simulation in the framework of the so-called *dynamical transport theory*, which has been recently proposed to deal, in a consistent manner, with anisotropic[16] as well as with inelastic[17] scattering mechanisms. In this theory the relaxation time is replaced by a collision time that depends on the orientation j of the applied electric field F_J. It can be shown that the collision time reduces to the classical relaxation time expression for isotropic and elastic scattering mechanisms (impurities, acoustical phonons, and carrier-carrier scattering), while, for anisotropic and elastic scattering centers (dislocations), Eq. (2.17) of Ref. 17 gives

$$\frac{1}{\tau_D(\mathbf{k})} = \frac{\pi e^2}{(2\pi)^3 \hbar} \int |V_{\mathrm{tot}}(q)|^2 \frac{q_j^2}{k_j^2} \delta_\alpha(\varepsilon_{k+q} - \varepsilon_k) d^3q, \tag{2.1}$$

where j is the external field direction and $V_{\mathrm{tot}}(q) = V_{\mathrm{tot}}(q,\omega=0)$ is the Fourier transform of the inelastic scattering potential $V_{\mathrm{tot}}(r,t) = V_{\pm\mathrm{tot}}(r,\omega)e^{i\omega t}$. For isotropic but inelastic scattering mechanisms (optical phonons) Eq. (2.18) of Ref. 17 gives

$$\begin{aligned}\frac{1}{\tau_D^{\pm}(\mathbf{k})} &= -B^{\pm} \frac{\pi e^2}{(2\pi)^3 \hbar} \int |V_{\pm\mathrm{tot}}(q,\omega_0)|^2 \frac{2k_j q_j}{k^2} \\ &\quad \times \delta_\alpha(\varepsilon_{k+q} - \varepsilon_k \mp \hbar\omega_0) d^3q \\ &\equiv \frac{-B^{\pm}}{\tau_B(k)},\end{aligned} \tag{2.2}$$

where

$$B^{\pm} = \mp \frac{f_0(\varepsilon_k \pm \hbar\omega_0) - f_0(\varepsilon_k)}{\hbar\omega_0 (\partial f_0/\partial\varepsilon)_{\varepsilon_k}}, \tag{2.3}$$

$f_0(\varepsilon)$ being the equilibrium occupation function. Note that Eq. (2.3) generates the result for elastic and isotropic center since $B^{\pm} = -1$ when $\omega_0 \to 0$. Since formula (2.2) directly connects the collision time to the classical relaxation time, the present simulation could be performed by extensively using the standard expressions of the relaxation time as, for instance, those described in the comprehensive work of Ridley,[18] in order to account for the ionized impurity, acoustical and optical phonon and carrier-carrier scattering mechanisms.

Concerning dislocations, the study of their role on the mobility of GaN is surprisingly restricted in the referred literature[10,11,13,14] to the so-called ''core effect'' scattering mechanisms though it is known for a long time that the dislocation strain field also prompts other scattering mechanisms through the deformation potential and the piezoelectric coupling.[16,19] We review briefly, in the following, the dislocation trapping and scattering properties that have been considered in our simulation. These properties will also be used to ground our model of barrier-controlled mobility in the last section of this paper.

B. Dislocation properties

1. Energy states

In ball and wire models, dislocations are defects whose core atoms (located along the dislocation line) do not possess the same number of first neighbors as atoms of the perfect crystal. Thus, at first sight, such core atoms may be seen as bearing dangling orbitals whose energy lies within the energy band gap and should confer to the dislocation some deep acceptor or donor character. However, a more fundamental analysis issues from *ab initio* calculations which unambiguously indicate that, for all the crystals studied[20–23] and more recently for GaN,[24] the dislocation core structure is fully reconstructed. This reconstruction results into the presence of shallow one-dimensional density of states lying below the conduction band or above the valence bands. A precise numerical calculation of such shallow states was undertaken in Ref. 25, in the framework of the envelope function approximation, by assuming that they originate from long-range binding potentials connected with the dislocation strain field through the deformation potential and piezoelectric potential coupling. In this approach, the ''*a*-edge'' threading dislocations in GaN (those that are mainly involved in the formation of subgrain boundaries of the columnar cell structure) should bind shallow electronic states lying at about 100 meV under the conduction band. Nevertheless, because of their Cottrell atmosphere (made up of segregated impurities or point defects), as-grown dislocations may also bind localized states through extrinsic mechanisms rather than because of the intrinsic properties noted above. Thus, the existence and location of dislocation energy states remain open questions, and we consider in the following such states and their energy E_{dislo} below the conduction band as being a free parameter for fitting our mobility measurements.

2. Dislocation state statistics

Forgetting about the one-dimensional band structure of the dislocation states, we may consider that all of these states

are, on average, located at a value E_{dislo} and closely spaced all along the dislocation line. Thus, it is clear that carriers trapped on such states interact electrostatically, increasing therefore the free energy of the whole system by an amount ΔF given by

$$\Delta F = n_t(E_{\text{dislo}} - E_F) + E_{\text{elec}}(n_t) - k_B T \ln[\Omega(n_t)], \tag{2.4a}$$

where n_t is the number of carriers trapped along the whole dislocation lines, E_F is the Fermi energy, $E_{\text{elec}}(n)$ is the electrostatic interaction energy of the trapped carriers (screening effects included), k_B is the Boltzmann constant, and T the absolute temperature. $\Omega(n_t) = D!/[(D-n_t)!n_t!]$ is the number of configurations leading to the distribution of n_t carriers among the D sites located along the dislocation lines. Various models can be used to calculate the screened interaction energy $E_{\text{elec}}(n_t)$ as, for instance, the concept of depleted region around the dislocation line[26] (as done for the study of Schottky diodes), or the usual Debye-Hückel screening.[27,28] Minimizing ΔF versus n_t leads to

$$\frac{\partial \Delta F}{\partial n_t} = 0 = E_{\text{dislo}} - E_F + \frac{\partial E_{\text{elec}}(n_t)}{\partial n_t} - kT \frac{\partial[\ln(\Omega(n_t)]}{\partial n_t}, \tag{2.4b}$$

where we have assumed that the dislocation energy state E_{dislo} does not depend on its occupation n_t (i.e., $\partial E_{\text{dislo}}/\partial n_t = 0$). Looking at an amphoteric dislocation (which can act as acceptor as well as donors) whose D sites may accommodate $2D$ electrons and introducing the occupation factor ξ corresponding to the neutral dislocation (so that the dislocation possess $2D\xi$ electrons when electrically neutral), then, the excess carrier n_t' trapped at the dislocation (and transforming it into a charged line) is given by

$$n_t' = 2D\left(\frac{1}{1+\exp\left(\dfrac{E_{\text{dislo}} + w(n_t) - E_F}{k_B T}\right)} - \xi\right), \tag{2.5}$$

where $w(n_t) = dE_{\text{elec}}(n_t)/dn_t$ is the derivative versus n_t of the screened electrostatic interaction energy between trapped carriers. Analytical expressions of $w(n_t)$ are standard. They may be found in Ref. 26 for the depleted region approximation or again in Refs. 27 and 28 for the Debye-Hückel screening approach. Slightly different expressions are obtained when the dislocation only provides donors or acceptor states instead of amphoteric states. In our calculation, expression (2.5) has been included in the neutrality equation in order to consider the dislocation trapping effect on the carrier statistics.

3. Core effect scattering

Formula (2.5) allows to determine the linear charge density $\lambda = n_t' e/Db$ of the dislocation lines, where b represents the distance separating neighboring traps along the dislocation line and e is the electron charge. This linear charge prompts a first scattering mechanism: the so-called ''core effect'' corresponding to the (screened) Coulomb potential associated with this linear charge and whose Fourier transform is obviously given by

$$V_{\text{Coulomb}}(q) = \frac{\lambda}{\varepsilon_0 \kappa(q) q^2}\, \delta(q_z) \tag{2.6}$$

for a dislocation lying along the O_z direction [which implies the presence of the $\delta(q_z)$ function]. $\kappa(q)$ stands for the static dielectric function used to account for screening effects. Note that this ''core effect'' is the only scattering mechanism that has been considered in the other studies on the role of dislocations in GaN.[10–14]

4. Long-range strain field scattering

Dislocations also provide other scattering mechanisms that are connected with their long-range strain field through the deformation potential and the piezoelectric coupling (in nonpolar materials). In direct-band-gap semiconductors, the deformation potential tensor $\boldsymbol{\Theta}$ associated with the conduction band reduces to a constant E_1 times a unit 3×3 matrix I so that if $\boldsymbol{\varepsilon}(\mathbf{q})$ represents the Fourier transform of the strain tensor, then the resulting deformation potential $V_{\text{DP}}(q)$ is given by $\boldsymbol{\Theta}:\boldsymbol{\varepsilon} = E_1 \mathbf{I}:\boldsymbol{\varepsilon} = E_1\,\text{Tr}(\varepsilon)$ where the symbol : indicates the contracted product of two tensors. Thus, the screened potential is

$$V_{\text{DP}}(q) = \Theta:\varepsilon(q)/\kappa(q) = [E_1/\kappa(q)]\text{tr}[\varepsilon(q)]. \tag{2.7}$$

In nonpolar materials, the piezoelectric coupling also occurs and may be deduced from the second Voigt equation $\mathbf{D} = \kappa\mathbf{E} + \mathbf{e}:\boldsymbol{\varepsilon}$, where $\mathbf{D}$ is the displacement vector, $\kappa = \varepsilon_0\varepsilon_L$ the material permitivity, $\mathbf{e}$ the piezoelectric tensor, and $\mathbf{E}$ the electric field. Since no net charge is introduced in the material by the dislocation strain field then $\text{div}(\mathbf{D}) = 0$. Thus $\text{div}(\kappa\mathbf{E}) = -\text{div}(\mathbf{e}:\boldsymbol{\varepsilon})$. Taking the Fourier transform of the latter expression, and introducing the dielectric function [as, for instance, the Debye-Hückel expression $\kappa(q) = \varepsilon_L(1 + k_{\text{DH}}^2/q^2)$ with $\mathbf{E} = -\text{grad}(V_{\text{piezo}})$] , we find

$$V_{\text{piezo}}(q) = i\,\frac{q[\mathbf{e}:\boldsymbol{\varepsilon}(q)]}{\varepsilon_0 \kappa(q) q^2}. \tag{2.8}$$

Note that for a dislocation lying along the O_Z axis, the Fourier transform of the strain field $\varepsilon(q)$ also contains a $\delta(q_z)$ function similar to the one that appears in Eq. (2.6).

In the particular case of GaN, the piezoelectric tensor is such that dislocations parallel to the c axis (in practice the threading dislocations) do not couple any piezoelectric potential.[28] However, we nonetheless introduced in our simulation the possibility that a given fraction of dislocations could have partially oblique orientations and induce some piezoelectric scattering potentials.

Finally, these strain field potentials were evaluated making use of the isotropic elastic medium approximation for the dislocation strain field determination. Such an approximation was shown to be sufficient in Ref. 29 and allows the use of the standard expressions of the dislocation strain field as those given in Ref. 30. The whole calculation has been done

TABLE I. Main parameters entering the numerical calculation, from Ref. 35.

Conduction effective mass m^*	0.20
Dielectric constants	$\varepsilon_L(\omega=0)=8.9,\ \varepsilon_L(\omega=\infty)=5.35$
Deformation potential	$E_1=8.3$ eV
Optical deformation potential	$D_0=6.12\times10^9$ eV/cm
Piezoelectric constants	$e_{33}=0.44,\ e_{31}=-0.22,\ e_{15}=-0.22$ C/m^2
Energy band gap	$E_G=3.39$ eV

using the Debye-Hückel dielectric function $\kappa(q)=\varepsilon_L(1+k_{\mathrm{DH}}^2/q^2)$, where $k_{\mathrm{DH}}^2=ne^2/(\varepsilon_0\varepsilon_L k_B T)$, for the determination of screened scattering potentials.

C. Theoretical results in terms of pure-diffusion mechanism

Simulation of the mobility in terms of pure-diffusion processes have been undertaken, including all the contributions recalled in the above subsections. The physical parameters used are the standard values found in literature (Table I). Some examples are given in Fig. 2 for a compensation ratio N_A/N_D arbitrarily chosen equal to 0.5. It shows a typical determination of the mobility versus temperature for various dislocation densities and for a donor density of $10^{18}\,\mathrm{cm}^{-3}$. It more particularly shows that dislocations mainly act as efficient scattering centers at low temperature. The high-temperature range is principally dominated by the ionized impurities as well as by optical phonon scattering. Nonetheless, dislocation densities larger than $10^{10}\,\mathrm{cm}^{-2}$ noticeably affect the mobility in the whole temperature range. Calculating the mobility versus carrier density at room temperature, whatever the density of dislocations and the position of their bound states, we are unable to reproduce the singular behavior shown Fig. 1: a model taking into account the effect of dislocations in terms of the pure-diffusion mechanism cannot produce the transport regime transition. This allows us to claim that this mobility collapse does not originate from pure-diffusion mechanisms even if dislocation properties (trapping and scattering mechanisms) are self-consistently considered in the simulation.

III. A DISLOCATION BARRIER MODEL

The idea of a barrier-controlled mobility has already been suggested for polycrystalline silicon films,[31] further extended to GaN in Ref. 32 and used in Ref. 33 to explain the thermally activated conductivity in undoped GaN layers. However, this kind of model is unable to explain the sharp mobility transition or again the existence of a critical carrier density at which it occurs. In our former approach,[6] the internal barriers associated with the walls of dislocations were supposed to have fixed height and were overcome by the carriers, because of a subsequent motion of the Fermi level when increasing the dopant density. Typically, such a model leads to a fixed critical density at which the sharp mobility transition occurs and which roughly corresponds to the transition between the nondegenerate to the degenerate electron gas behavior when increasing the dopant density (i.e., at a value laying near the intrinsic conduction band density of states at about $\sim 2\times10^{18}\,\mathrm{cm}^{-3}$). Thus, it was impossible to explain why this critical carrier density value would depend on the defect substructure and could be as low as $2\times10^{17}\,\mathrm{cm}^{-3}$ as obtained in the second series of GaN layers (series Ω) presented in Fig. 1.

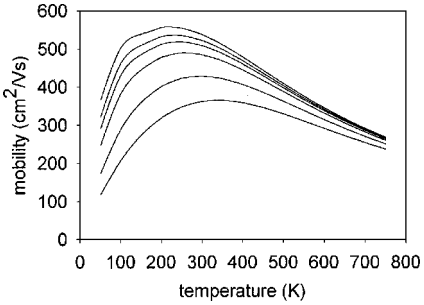

FIG. 2. Carrier mobility versus temperature for various dislocations densities. From the top to the bottom, curves are obtained with $N_{\mathrm{dislo}}=0$ (no dislocation), 5×10^9, 10^{10}, 2×10^{10}, 5×10^{10}, and $10^{11}\,\mathrm{cm}^{-2}$. In all the cases, the compensation ratio N_A/N_D is 0.5 and the donor density is $10^{18}\,\mathrm{cm}^{-3}$.

In the present model, we suppose that dislocations are responsible for localized energy states closely spaced all along their line. Because of a large density of states, such levels are attracted, at equilibrium, by the Fermi level and, in the rigid shift approximation, a resulting band bending occurs around the dislocation line, in a way similar to what happens in the depleted region of a Schottky diode. This shift corresponds in fact to the quantity $w(n)$ introduced previously. Reversing Eq. (2.5), it is given by

$$w(n_t')=E_F-E_{\mathrm{dislo}}+k_BT\ln\left(\frac{1-\xi-n_t'/2D}{\xi+n_t'/2D}\right). \qquad (3.1)$$

However the ratio $n_t'/2D$ is generally very small so that using an occupation factor of about 0.5 for the neutral dislocation, the $w(n_t')$ quantity is approximately equal to the difference between the Fermi level and the neutral dislocation binding energy E_{dislo}. Figure 3 illustrates such a band bending.

The band bending shape $E_C(r)$ may be found by assuming that, within a given radius R, the area surrounding the dislocation line is depleted. Then, using the following boundary conditions $E_C(0)=E_F-E_{\mathrm{dislo}}$ and $E_C(R)=0$, Poisson's equation around the dislocation line is given by

$$\Delta V=\frac{1}{r}\frac{d}{dr}\left(r\frac{dV}{dr}\right)=-\frac{(N_D-N_A)e}{\varepsilon_0\varepsilon_L} \qquad (3.2)$$

and with $E_C(r)=-eV(r)$, its integration leads to

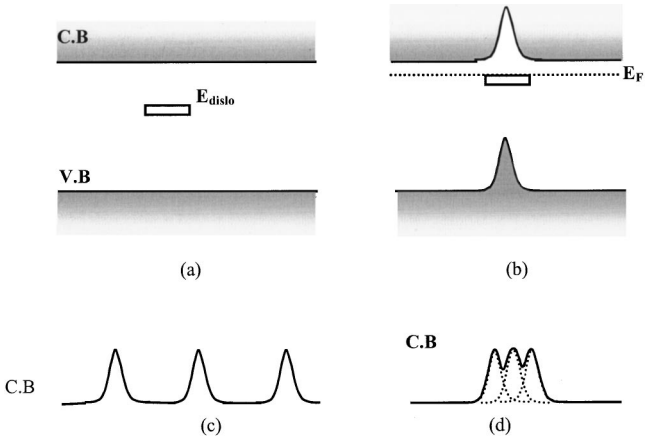

FIG. 3. Schematic representation of the dislocation induced band bending of the conduction band. (a) represents a neutral dislocation; (b) represents a negatively charged dislocation with energy levels shifted towards the Fermi energy level. (c) represents individual dislocations. (d) 3*d* represents a barrier induced by dislocations.

$$E_C(r)=\begin{cases}(E_F-E_{\text{dislo}})-\dfrac{k_BTr^2}{4\lambda^{*2}} & \text{for } r<R\\ 0 & \text{for } r>R,\end{cases} \tag{3.3}$$

while $E_C(R)=0$ leads to

$$R=2\lambda^*\sqrt{\frac{E_F-E_{\text{dislo}}}{k_BT}}, \tag{3.4}$$

where $\lambda^*=\sqrt{\varepsilon_0\varepsilon_L k_BT/(N_D-N_A)e^2}$. Note that λ^* formally differs from the classical Debye-Hückel screening wavelength given by $\lambda_{\text{DH}}=\sqrt{\varepsilon_0\varepsilon_L k_BT/ne^2}$ where $n=N_D^+-N_A^--n_t$.

We consider now a family of neighboring dislocations belonging to a subgrain boundary (one dislocation wall). Such dislocations should result into the existence of internal electronic barriers as long as the mean distance *d* separating two neighboring dislocations would be smaller than $2R$ [Fig. 3(d)], otherwise dislocations may be considered as independent scattering centers [Fig. 3(c)]. Thus, a rough criterion that separates the barrier-controlled mobility from a pure-diffusion process is

$$d<2R=4\lambda^*\sqrt{\frac{E_F-E_{\text{dislo}}}{k_BT}}\rightarrow\text{barrier-controlled mobility.} \tag{3.5}$$

When $d<2R$, the energy at the saddle point E_{spt} of the barrier, localized between two neighboring dislocations, is given by

$$E_{\text{spt}}=2E_C(d/2)=2\left((E_F-E_{\text{dislo}})-\frac{k_BT}{16}\frac{d^2}{\lambda^{*2}}\right), \tag{3.6}$$

while its thickness d_{spt} is approximately given by

$$d_{\text{spt}}=2\sqrt{R^2-\frac{d^2}{4}}. \tag{3.7}$$

Obviously, a lot of other more or less refined estimates of the saddle-point characteristics can be obtained but, in practice, they lead to quite identical final results.

One can already notice that relation (3.5) permits us to define a simple rule of thumb for a fast estimate of the critical free carrier density at which the steep transition in transport regime occurs: the ratio d/R_{critical} is quite constant (if the dependence of E_F-E_{dislo} versus *n* is neglected) or, equivalently, the product $n_{\text{critical}}d^2$ is quite constant. For instance, one can anticipate, before making any calculation, that for the two series presented in Fig. 1, the series α presents dislocation spacing that is on average 2 times lower than the one for series Ω, which would be consistent with the fact that the crystalline quality is improved from the first series to the second. At the limit, an extreme behavior would be met for GaN layers grown in optimum conditions such that there is no marked grain boundaries (as for instance in atmospheric pressure MOVPE): a series of such layers should not display any transition in the electrical transport regime nor any mobility collapse.

So let us now approximate the barrier saddle point to a squared potential barrier of energy height E_{spt} and thickness d_{spt}. We assign to this point a tunnel transmission power $T(\varepsilon)$ whose expression can be found in any textbook. In a material free of energy barriers, each carrier of energy $\varepsilon(k)$ statistically contributes to the final conductivity through the elemental contribution to the current density $j_k=e\,\delta f_k v_k$, where $v_k=\hbar k/m^*$ is the carrier velocity. δf_k is the modification brought to the Fermi-Dirac occupation function of state *k* by the applied external field F_{appl}. As soon as such a carrier meets a potential barrier, it contributes, in fact, to the whole current by the effective elemental contribution $j_k^*=T(\varepsilon_k)j_k$. Thus, the whole current density in the presence of barriers is given by

$$j^*=2e\int T(\varepsilon_k)\,\delta f_k v_k n_k d^3k, \tag{3.8}$$

where n_k is the *k* density of states and where a factor 2 is introduced to account for the two possible spin values. Then, δf_k is classically given by

$$\delta f_k=-\left(\frac{\partial f_0}{\partial\varepsilon}\right)_k\tau_D(k)v_kF_{\text{appl}}, \tag{3.9}$$

where, in the framework of the dynamical theory, the collision time $\tau_D(k)$ given by formula (2.1) replaces the standard relaxation time. Integrating Eq. (3.8) and defining the carrier mobility μ by the relation $j=ne^2\mu F$, one obtains the mobility versus carrier density evolution.

IV. DONOR STATISTICS

The above section clearly shows that our model strongly depends on the location of the Fermi energy E_F, which is determined by solving the neutrality equation

$$n=N_D^+-N_A^--n_t, \tag{4.1}$$

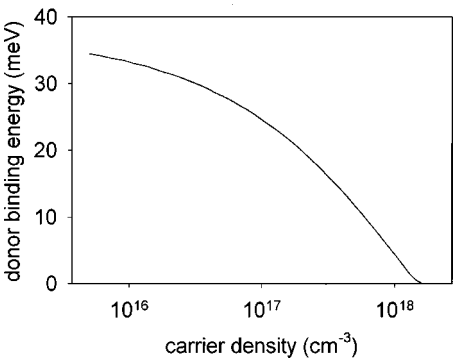

FIG. 4. Impurity binding energy vs the donor density in the hydrogenic impurity model calculated with $m_C^*=0.22m_0$ and $\varepsilon_L=8.9$.

where n is the free carrier density in the conduction band, N_D^+ the density of ionized donors, N_A^- the density of ionized compensating acceptors, and n_t the density of electrons trapped at the dislocation line given by expression (2.5). Therefore, the Fermi-level position is strongly dependent on the way the donor statistics is described.

The experimental results shown in Fig. 1 range from a region where the material is moderately doped towards a region where it is ''heavily'' doped. Various physical consequences arise from this fact and introduce some complexity in the theoretical description of the donor statistics.

(i) As the dielectric response will also increase with the carrier density, this should result in a decrease of the donor binding energy. To account for this effect and calculate the binding energy E_D versus carrier density, we used the following simple argument as suggested by Bonch-Bruyevich in Ref. 34. In the unscreened hydrogenic model, the Hamiltonian $p^2/2m^*-e^2/\varepsilon_L r$ leads to an energy $E_D(r)=\hbar^2/2m^*r^2-e^2/\varepsilon_L r$ for a carrier at r from the donor. Its minimum reached for $r^*=\hbar^2\varepsilon_L/m^*e^2$ corresponds to $E_D(r^*)=-m^*e^4/2\hbar^2\varepsilon_L^2$. In the case of a screened hydrogenoid Hamiltonian $p^2/2m^*-e^{-r/\lambda_{\mathrm{DH}}}e^2/\varepsilon_L r$, the same procedure can only be performed numerically. Results are shown in Fig. 4. They clearly indicate that the donor binding energy $E_D(n)$ vanishes for n values larger than $\sim 1.5\times 10^{18}\,\mathrm{cm}^{-3}$ for $m_C^*=0.22m_0$ and $e_L=8.9$.

(ii) It is then tempting to introduce $E_D(n)$ in the standard expression of the ionized donor density given by

$$N_D^+=\frac{N_D}{1+ge^{[E_F-E_D(n)]/k_BT}}, \tag{4.2}$$

where g is the donor level degeneracy ($g=2$), and then simply numerically solve Eq. (4.1) considering the results shown Fig. 4. This being done, the carrier concentration with increasing donor density N_D is found to progressively saturate so that, in practice, it is impossible to obtain any carrier density without introducing unrealistic (too large) values of N_D. It is clear, however, that expression (4.2) can no longer be used when the material starts being heavily doped since phenomena other than screening effects occur in parallel such as the appearance of an impurity band as soon as the crystal impurity radius r^* (corresponding to the minimum of the donor energy) becomes of the same order of magnitude as the mean distance between impurities. Some conduction-band tailing occurs and must also be considered. To overcome these points, we have considered that the spreading of the donor density of states could be described by the following Gaussian function:

$$N_D(E)=N_D\frac{1}{\sigma\sqrt{\pi}}e^{-[(E-E_D)/\sigma]^2}, \tag{4.3}$$

where N_D is the donor density and σ is a parameter representing typically the dispersion in the interaction energy between a bound carrier and its randomly distributed neighbors. Its order of magnitude correspond to a fraction γ of the interaction between a bound electron and the neighboring impurities (Coulomb, exchange, and correlation potentials). In this paper, this term is *arbitrarily* chosen as

$$\sigma=\gamma\frac{e^2}{4\pi\varepsilon_0\varepsilon_L a}, \tag{4.4}$$

where $a\approx(N_D)^{-1/3}$ represents the mean spacing between impurities. It is noteworthy to see that γ accounts for the dispersion in the impurity spatial distribution and, consequently, is likely to vary from one growth process to the other. It is clear that low doping leads to small σ values. In such cases, the Gaussian function acts as a Dirac function of width σ so that

$$\lim_{\sigma\to 0}N_D(E)=N_D\delta(E-E_D). \tag{4.5}$$

To account for the conduction-band tailing, we have considered that the conduction-band edge would spread down to a value $E^*=E_C-\zeta$, where ζ has an equivalent meaning to that of our first parameter σ. For the sake of simplicity we have taken $\zeta=\sigma$ in the numerical computation.

For energy values E larger than E^*, the impurity states described by Eq. (4.3) would be in resonance with the conduction band, giving rise to free carriers, while impurity states whose E value is lower than E^* remain localized states that can only be ionized because of the thermal energy. With the above points, the full ionized donor density is finally given by

$$\begin{aligned}N_D^+&=\int_{E^*}^{\infty}N_D(E)dE+\int_{\infty}^{E^*}N_D(E)f_D(E)dE\\&=\frac{N_D}{2}\mathrm{erfc}\left(\frac{E^*-E_D}{\sigma}\right)+\frac{N_D}{\sigma\sqrt{\pi}}\int_{-\infty}^{E^*}\frac{e^{[(E-E_D)/\sigma]^2}}{1+ge^{(E_F-E)/k_BT}}dE,\end{aligned} \tag{4.6}$$

where erfc is the complementary error function. It is worth noticing that the limit of Eq. (4.6), when σ tends towards zero (low doping), corresponds exactly to expression (4.2). Contrarily, for extremely large dopant densities, $E_D(n)$ equals zero and expression (4.6) affirms that practically all the N_D donors are automatically ionized. The above approach is only intuitively grounded. It must be considered as a way to get a continuous description of the donor statistics

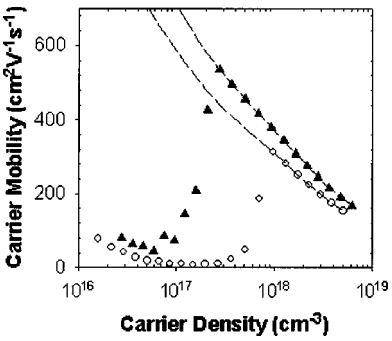

FIG. 5. Modeling of the mobility versus carrier density obtained at 300 K for two different distances between neighboring dislocations in order to fit the experimental curves corresponding to series α and Ω in Fig. 1: open circles: $d=380$ Å and a compensation ratio equal to 0.4. Full triangles: $d=650$ Å with a compensation ratio equal to 0.3. The dashed lines represent the mobility obtained with the same dislocation densities and same compensation ratios but in terms of pure-diffusion processes (no ''wall effect'').

ranging from moderate to heavily doping. We have arbitrarily chosen $\gamma=1$ in the numerical application.

V. THEORETICAL RESULTS

Using this model, we are able *to quantitatively reproduce the steep transition* of the mobility-density plot taking realistic parameters for the dislocation densities and their mean spacing in the dislocation walls (as obtained from TEM observations). Figure 5 shows two theoretical curves that can fit the experimental trends presented in Fig. 1. The values for the high-mobility regime have been intentionally chosen slightly higher in order to account for the fact that the experimental Hall mobility is slightly lower than the free carrier mobility (see, for instance, Ref. 5). The two dashed lines represent for each case the mobility that would have been obtained with the same dislocation densities, randomly distributed, without considering their collective effect when partially organized into dislocation walls. It appears clearly that the distance of neighboring dislocations in the subgrain boundaries needs to be increased almost double in order to account for a shift of the collapse by a factor of 4 between α and Ω series: typically the average spacing of dislocations in the series α should be chosen equal to 38 nm and for the series Ω, 65 nm. The compensation ratio has to be chosen slightly higher for the series α than for the better quality series Ω (0.4 and 0.3, respectively). The dislocation densities needed for the fit have been, respectively, taken equal to 5×10^{9} and $2\times10^{10}\,\mathrm{cm}^{-2}$, in agreement with the TEM estimates.[5,9] The location of the dislocation level under the conduction band turns out to be a sensible parameter that determines the mobility value and behavior in the low-mobility range. The better fit of the experimental results shown in Fig. 1 corresponds to a location at about 200 meV under the conduction band. Such a value noticeably differs from that (100 meV) found in Ref. 23 using intrinsic arguments. It may be a clue that as-grown dislocation levels do result from an extrinsic decoration of the dislocation line by some impurities or point defects.

Obviously other possible experimental trends can be found and forecast for some other choice of the compensation ratio, other dislocation densities, etc., in order to fit other series of layers. For instance, a nonoptimum epilayer growth temperature may favor the growth of more compensated layers because of unwanted carbon incorporation,[8] and this may result in a series of points laying on another curve but the collapse position should not change at all as the distribution of dislocation has not changed. Here it appears again clearly that the study of the mobility collapse is a valuable tool for the assessment of material quality.[9]

VI. CONCLUSION

Inserting a comprehensive list of scattering mechanisms (ionized impurities, acoustical and optical phonons, carrier-carrier scattering) and including all the characteristics of dislocation trapping and scattering mechanisms in our low-field transport simulation code, it was impossible to find any configuration leading to a good description of the experimental behavior of the mobility versus the carrier concentration in terms of pure-diffusion mechanisms. Instead, we paid attention to the dislocation substructure mainly built up of dislocation walls (subgrain boundaries). Assuming that the dislocation density of states is responsible for some band bending around the dislocation lines, we could deduce a condition indicating when the carrier mobility is either controlled by internal electronic barriers (as long as the dielectric response of the material remains unable to separate the band bending of neighboring dislocations) or would simply correspond to some diffusion processes associated with independent dislocations. Such a model fits quite well the mobility collapse observed as the carrier density is reduced in columnar cell GaN samples and clearly illustrates the importance of the role of the dislocation spatial distribution (the defect ''substructure''), which, to our best knowledge, is generally neglected in similar dislocation problems. Finally, it allows us to claim that dislocations are, at least in our samples, responsible for an extrinsic linear density of states on average localized at about 200 meV under the conduction band.

[1] V. W. L. Chin, T. L. Tanley, and T. Osotchan, J. Appl. Phys. **75**, 7365 (1994).
[2] B. K. Ridley, J. Appl. Phys. **84**, 4020 (1998).
[3] B. K. Ridley, J. Phys.: Condens. Matter **10**, 6717 (1998).
[4] Subhabrata Dhar and Subhasis Ghosh, J. Appl. Phys. **86**, 2668 (1999).
[5] Z. Bougrioua, J.-L. Farvacque, I. Moerman, P. Demeester, J. J. Harris, K. Lee, G. Van Tendeloo, O. Lebedev, and E. J. Thrush, Phys. Status Solidi B **216**, 571 (1999).
[6] J. L. Farvacque, Z. Bougrioua, I. Moerman, G. Van Tendeloo, and O. Lebedev, Physica B **273-274**, 140 (1999).
[7] W. van der Stricht, I. Moerman, P. Demeester, J. A. Crawley, E.

J. Thrush, P. G. Middelton, C. Trager-Cowan, and K. O'Donnell, in *Gallium Nitride and Related Materials*, edited by F. A. Ponce, MRS Symposia Proceedings No. 395 (Materials Research Society, Pittsburgh, 1996), p. 231.

[8] Z. Bougrioua, I. Moerman, P. Demeester, E. J. Trush, J.-L. Guyaux, and J.-C. Garcia, Proceedings of the Eighth European Workshop on MOVPE, Prague (Czech Republic) (The Institute of Physics ASCR, Prague, 1999), p. 61.

[9] Z. Bougrioua, I. Moerman, N. Sharma, R. H. Wallis, J. Cheyns, K. Jacobs, E. J. Thrush, L. Considine, R. Beanland, J.-L. Farvacque, and C. Humphreys, J. Cryst. Growth (to be published).

[10] N. G. Weimann, L. F. Eastman, D. Doppalapudi, H. M. Ng, and T. D. Moustakas, J. Appl. Phys. **83**, 3656 (1998).

[11] H. M. Ng, D. Doppalapudi, T. D. Moustakas, N. G. Weimann, and L. F. Eastman, Appl. Phys. Lett. **73**, 821 (1998).

[12] J. D. Albrecht, P. P. Ruden, E. Bellotti, and K. F. Brennan, MRS Internet J. Nitride Semicond. Res. **4**, G6.6 (1999).

[13] D. C. Look and J. R. Sizelove, Phys. Rev. Lett. **82**, 1237 (1999).

[14] H. Tang, J. Webb, J. Bardwell, B. Leathem, S. Charbonneau, and S. Raymond, J. Electron. Mater. **29**, 268 (2000).

[15] K. Seeger, in *Semiconductor Physics* (Springer, Wien, 1973), p. 202.

[16] J.-L. Farvacque, Semicond. Sci. Technol. **18**, 914 (1995).

[17] J.-L. Farvacque, Phys. Rev. B **62**, 2536 (2000).

[18] B. K. Ridley, *Quantum Processes in Semiconductors*, 3rd ed. (Clarendon, Oxford, 1993).

[19] Z. Bougrioua, D. Ferre, and J-L. Farvacque, J. Appl. Phys. **79**, 1536 (1996); G. Faivre and G. Saada, Phys. Status Solidi B **52**, 127 (1972); L. Merten, Phys. Kondens. Mater. **2**, 53 (1964); D. L. Dexter and F. Seitz, Phys. Rev. **86**, 964 (1952).

[20] A. Umerski and R. Jones, Philos. Mag. A **67**, 905 (1992).

[21] R. Jones, A. Umerski, P. Sitch, M. I. Heggie, and S. Öberg, Phys. Status Solidi A **137**, 389 (1993).

[22] P. K. Sitch, R. Jones, S. Öberg, and M. I. Heggie, Phys. Rev. B **50**, 17 717 (1995).

[23] P. K. Sitch, R. Jones, S. Öberg, and M. I. Heggie, J. Phys. III **7**, 1381 (1997).

[24] J. Elsner, R. Jones, M. I. Heggie, P. K. Sitch, M. Haugk, Th. Frauenheim, S. Oberg, and P. R. Briddon, Phys. Rev. B **58**, 12 571 (1998).

[25] J.-L. Farvacque and Ph. François, Physica B **273-274**, 995 (1999).

[26] W. T. Read, Philos. Mag. **45**, 335 (1954); **45**, 1119 (1954).

[27] R. A. Masut, C. Penchina, and J.-L. Farvacque, J. Appl. Phys. **53**, 4864 (1982); R. Labusch and W. Schröter, *Dislocations in Solids* (North-Holland, Amsterdam, 1980), Vol. 5, p. 129.

[28] C. Shi, P. M. Asbeck, and E. T. Yu, Appl. Phys. Lett. **74**, 573 (1999).

[29] D. Vignaud, J.-L. Farvacque, and D. Ferré, Phys. Status Solidi **2**, 110 (1982).

[30] See, for instance, J. P. Hirth and J. Lothe, *Theory of Dislocations* (McGraw-Hill, New York, 1968).

[31] J. Y. W. Seto, J. Appl. Phys. **46**, 5247 (1975).

[32] M. Fehrer, S. Einfeldt, U. Birkle, T. Gollnik, and D. Hommel, J. Cryst. Growth **189/190**, 763 (1998).

[33] J. Salzman, C. Uzan-Saguy, R. Kalish, V. Richter, and B. Mayler, Appl. Phys. Lett. **76**, 1431 (2000).

[34] V. L. Bonch-Bruyevich, *The Electronic Theory of Heavily Doped Semiconductors* (Elsevier, New York, 1966), Chap. 4.

[35] A compilation of GaN parameters with references can be found at http://www.iiiv.cornell.edu/www/foutz/nitride.html